

Look Before You Fuse: 2D-Guided Cross-Modal Alignment for Robust 3D Detection

Xiang Li

University of Science and Technology of China
xiangli@mail.ustc.edu.cn

Abstract

Integrating LiDAR and camera inputs into a unified Bird’s-Eye-View (BEV) representation is crucial for enhancing 3D perception capabilities of autonomous vehicles. However, current methods are often affected by misalignment between camera and LiDAR features. This misalignment leads to inaccurate depth supervision in camera branch and erroneous fusion during cross-modal feature aggregation. The root cause of this misalignment lies in projection errors, stemming from minor extrinsic calibration inaccuracies and rolling shutter effect of LiDAR during vehicle motion. In this work, our key insight is that these projection errors are predominantly concentrated at object-background boundaries, which are readily identified by 2D detectors. Based on this, our main motivation is to utilize 2D object priors to pre-align cross-modal features before fusion. To address local misalignment, we propose **Prior Guided Depth Calibration (PGDC)**, which leverages 2D priors to correct local misalignment and preserve correct cross-modal feature pairs. To resolve global misalignment, we introduce **Discontinuity Aware Geometric Fusion (DAGF)** to process calibrated results from PGDC, suppressing noise and explicitly enhancing sharp transitions at object-background boundaries. To effectively utilize these transition-aware depth representations, we incorporate **Structural Guidance Depth Modulator (SGDM)**, using a gated attention mechanism to efficiently fuse aligned depth and image features. Our proposed method achieves state-of-the-art performance on nuScenes validation dataset, with its mAP and NDS reaching 71.5% and 73.6% respectively.

Introduction

Robust 3D perception is a cornerstone of autonomous driving, where the effective fusion of complementary sensors like cameras and LiDAR is essential. For instance, images provide rich semantic representations but lack accurate depth information. Conversely, point clouds deliver precise geometric and depth cues but suffer from sparsity and absence of semantic context. Thus, effectively harnessing the complementary strengths of multi-modal data while addressing their inherent limitations is critical for building robust perception systems.

While promising, the fusion of LiDAR and camera data introduces significant challenges, primarily stemming from

Copyright © 2026, Association for the Advancement of Artificial Intelligence (www.aaai.org). All rights reserved.



Figure 1: Projection errors misplace distant points from the wall (cyan/green) onto the foreground car (which should be red). In contrast, background points, like those on the wall (orange) and garage (blue), are projected correctly, clearly defining the boundary between them. This highlights the system’s failure to handle sharp foreground-background depth changes, which can be efficiently captured by 2D detectors.

inherent cross-modal misalignment. Specifically, the inherent misalignment between point cloud and image creates obstacles that undermine the effectiveness of multi-sensor fusion (Yu et al. 2023). For example, a fundamental challenge in BEV perception lies in recovering the implicit depth information from 2D images to generate precise BEV feature representations for downstream neural networks. And therefore, a variety of approaches have focused on leveraging LiDAR signals to provide explicit depth supervision (Li et al. 2023) or develop implicit fusion methods that integrate camera and LiDAR information to implicitly provide depth information (Liu et al. 2023; Liang et al. 2022). Nevertheless, the misalignment of point cloud and image features due to calibration errors remains an insufficiently addressed problem, which leads to two major issues. First, the misalignment between the camera and LiDAR sensors leads to missing or erroneous depth supervision, degrading depth estimation accuracy, especially in areas of dramatic depth variation. Second, during the information fusion process, incorrect geometry-camera pairings can confuse the fusion mod-

ule, making effective integration particularly challenging.

Existing approaches have attempted to mitigate cross-modal misalignment, yet each suffers from significant drawbacks. To ensure feature consistency, some methods like ObjectFusion (Cai et al. 2023) adopt an object-centric strategy to avoid direct projection errors. While this effectively sidesteps the main cause of misalignment, it comes at the cost of sacrificing crucial contextual information. Other approaches like MetaBEV (Ge et al. 2023) and RobBEV (Wang et al. 2024) attempt to mitigate misalignment effects by designing more robust and adaptive fusion modules. Although these modules are more resilient to inconsistent inputs, they cannot correct the initial geometric errors from the view transformation. In essence, they are skillfully fusing features that have already been misplaced. Finally, global alignment techniques like GraphBEV (Song et al. 2024a) directly address the geometric problem, effectively eliminating misalignment in areas with steep depth gradients. However, they tend to unnecessarily smooth geometrically stable regions where misalignment is negligible or even entirely absent, thereby incorrectly modifying already-correct depth values.

These methods ignore the fact that misalignment stems from two primary sources, both of which cause projection errors that are amplified with increasing depth: minor extrinsic calibration errors and motion-induced distortions from the LiDAR’s rolling shutter effect. These projection errors are minor for points on nearby objects but become significant for points on distant background, creating a severe misalignment of features at their shared boundaries. Targeting the root causes of misalignment, we propose a framework that uses 2D priors to guide geometric correction and mitigate misalignment. Our core insight is that critical errors predominantly occur at the boundaries between foreground objects and background regions where depth changes sharply, as illustrated in Figure 1.

In this paper, we introduce three synergistic modules. First, to address the misalignment problem at its root, we propose **(1) Prior Guided Depth Calibration (PGDC)**. Our core philosophy, “Look Before You Fuse”, proposes that instead of attempting to sort out already-misaligned data, we should in advance correct it using high-level semantic guidance. PGDC actively uses 2D detection proposals as explicit geometric priors to locate and correct misaligned point cloud data, providing a significantly more accurate depth map to supervise the camera branch’s depth estimation. However, a corrected sparse map alone is not enough. To enable the network to fully understand the scene’s geometric structure, we introduce **(2) Discontinuity Aware Geometric Fusion (DAGF)**. Rather than using the raw depth map, DAGF processes it to create a dense and structurally aware representation by suppressing noise and explicitly enhancing sharp transitions at object boundaries. This enhanced representation, which encodes both reliable geometry and critical boundary information, is then fused with camera features, providing direct and unambiguous geometric guidance to reduce artifacts in final BEV output. To effectively utilize these calibrated signals for the view transformation, we introduce the **(3) Structural Guidance Depth**

Modulator (SGDM). This module intelligently fuses image features and dense geometric representation from DAGF using a gated attention mechanism. Its purpose is to predict a highly accurate depth distribution for each pixel, enabling a more precise projection of features into the final BEV space.

Our contributions are summarized below:

- We reveal that feature misalignment predominantly occurs at object-background boundaries and propose **Prior Guided Depth Calibration (PGDC)**, a novel module that actively uses 2D priors to locate and resolve such misalignment, thereby providing more accurate depth supervision. To our best knowledge, our work is the first to use 2D detection results as explicit guidance for correcting cross-modal geometric inconsistencies before fusion.
- Capitalizing on the intrinsic correlation between depth discontinuities and object-background boundaries, we introduce the **Discontinuity Aware Geometric Fusion (DAGF)** module that explicitly optimizes cross-modal feature alignment through discontinuity-aware mechanisms, significantly improving geometric consistency in multi-sensor perception.
- We introduce the **Structural Guidance Depth Modulator (SGDM)**, an efficient attention-based module that fuses calibrated visual and geometric cues to generate a highly accurate depth distribution for view transformation.
- Extensive experiments are conducted on the nuScenes Dataset, and our method achieves state-of-the-art performance on the nuScenes validation dataset with mAP and NDS of 71.5% and 73.6%.

Related Work

LiDAR-only 3D Object Detection. LiDAR-based 3D detection methods are categorized by their data representation. Point-based methods (Qi et al. 2017, 2018; Li, Wang, and Wang 2021) process raw point clouds with MLPs. Voxel-based methods (Liu et al. 2024a; Chen et al. 2023; Zhou and Tuzel 2018) use sparse 3D convolutions on discretized grids, with efficient pillar-based variants (Lang et al. 2019) using 2D backbones. Point-voxel hybrid methods (Song et al. 2023b; Miao et al. 2021) combine both for higher accuracy at the cost of greater computational overhead.

Camera-only 3D Object Detection. Camera-based 3D detection has shifted toward multi-view systems (Zhang et al. 2025; Wang et al. 2022), which outperform monocular methods (Lu et al. 2021; Pu et al. 2025) but increase computational complexity. The Lift-Splat-Shoot (LSS) (Phillion and Fidler 2020) paradigm, which projects image features into 3D using depth estimation, is a key development. This has inspired frameworks that use LiDAR for depth supervision (Reading et al. 2021), such as BEVDet (Huang and Huang 2022), and other techniques that distill LiDAR information (Guo and Ling 2025).

LiDAR-camera fusion 3D Object Detection. Multi-modal fusion is now the standard for 3D object detection. Fusion strategies have evolved from early point-level methods that augment raw LiDAR points with image features (Yin, Zhou,

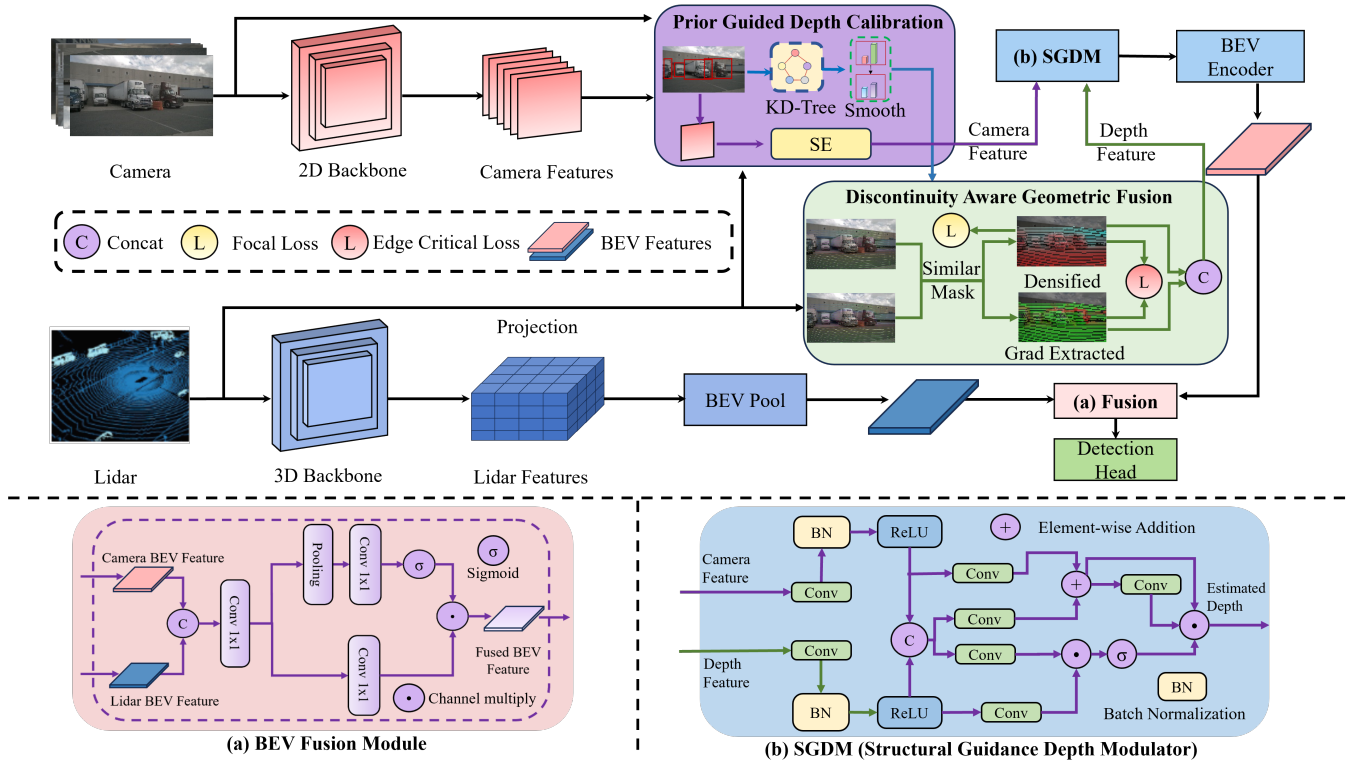


Figure 2: Overview of our proposed framework. It introduces two core modules, Prior Guided Depth Calibration (PGDC) and Discontinuity Aware Geometric Fusion (DAGF), to proactively mitigate multi-sensor feature misalignment before view transformation. Fusing the calibrated camera BEV features with LiDAR BEV features leads to robust 3D detection.

and Krähenbühl 2021; Liu et al. 2022; Wang et al. 2021), to more advanced feature-level approaches that use attention mechanisms to integrate 3D proposals with image features (Song et al. 2024b, 2023a; Chen et al. 2022). The current state-of-the-art primarily uses BEV-based fusion (Cai et al. 2023; Ge et al. 2023; Liang et al. 2022; Song et al. 2024a), which unifies both modalities in a shared bird’s-eye-view space for more efficient and robust cross-modal interaction.

Method

Framework Overview

As shown in Figure 2, our proposed framework is a multi-sensor fusion pipeline built upon the strong BEVFusion (Liang et al. 2022) baseline, designed to explicitly mitigate feature misalignment in Bird’s Eye View (BEV) perception. The framework processes inputs from a set of N surround-view cameras and a 360-degree LiDAR sensor. Our contribution is a framework of three synergistic modules. First, **Prior Guided Depth Calibration (PGDC)** uses 2D bounding boxes to correct misaligned LiDAR points at object boundaries, outputting a refined sparse depth map and enhanced image features. Second, **Discontinuity Aware Geometric Fusion (DAGF)** uses the corrected depth to generate a dense representation that captures reliable geometric structure. Finally, the **Structural Guidance Depth Modulator (SGDM)** fuses the enhanced image features (from PGDC)

and the dense geometric representation (from DAGF) to predict a depth distribution for each camera view. Following the Lift-Splat-Shoot (LSS) paradigm, these are projected into a unified BEV feature map, which is then fused with LiDAR BEV features to produce robust 3D detection results.

Prior Guided Depth Calibration (PGDC)

As shown in Figure 3, the Prior Guided Depth Calibration (PGDC) module operates independently on each of the N camera views to correct the initial sparse depth supervision derived from LiDAR. For each view $i \in \{1, \dots, N\}$, the inputs are the image features $F_{\text{img}}^{(i)} \in \mathbb{R}^{H \times W \times C}$ and the corresponding sparse depth map $D_{\text{raw}}^{(i)} \in \mathbb{R}^{H \times W}$, which is generated by projecting the LiDAR point cloud into that camera’s image plane.

First, a 2D detection head provides a set of bounding boxes $\{B_j^{(i)}\}$ for each image. Based on our observation that misalignment is concentrated at object boundaries, we use these boxes to isolate critical regions. For each box $B_j^{(i)}$, we filter the LiDAR points whose projections fall within it. To mitigate misalignment, we introduce a novel smoothing operation detailed in Algorithm 1. Instead of simple averaging, our method captures the local depth structure more effectively. For each LiDAR point projected to a pixel p with depth d_p , we first use a KD-Tree to find its 10 nearest neighbors, \mathcal{N}_p . We then select the two neighbors with the

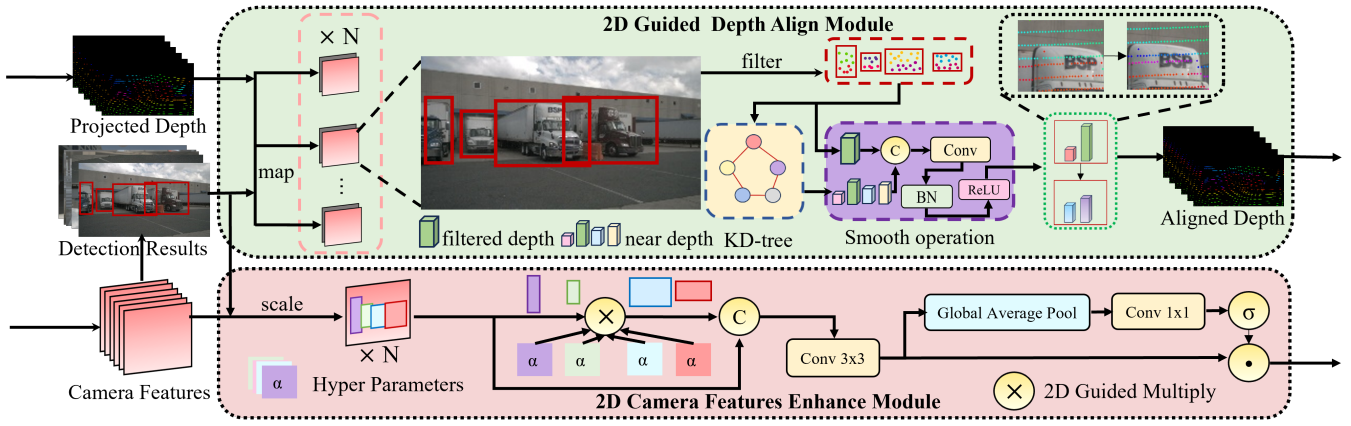


Figure 3: The **Prior Guided Depth Calibration (PGDC)** module leverages 2D detection boxes as priors to precisely target and correct the most severe feature misalignments, which are caused by calibration errors and motion distortion. By applying localized smoothing to the point cloud within these detected regions, the module corrects the erroneous depth supervision signal. Simultaneously, it enhances the features of these critical image areas.

smallest depth and the two with the largest depth, forming a set of four critical neighbors, $\mathcal{N}_{\text{critical}} \subset \mathcal{N}_p$. This selection strategy is designed to simultaneously capture the object’s own depth consistency (via the nearest points) and the sharp depth discontinuity at the boundary between the object and the background (via the farthest points), thereby preserving critical information while smoothing noise. The depth of the original point is concatenated with the depths of these four selected neighbors, creating a 5-channel feature map, f_p , for that pixel:

$$f_p = \text{concat}(d_p, \{d_q\}_{q \in \mathcal{N}_{\text{critical}}}) \quad (1)$$

This feature map is then processed through a lightweight convolutional block—consisting of a Convolution, Batch Normalization, and a ReLU activation—to produce the final single-channel, smoothed depth value:

$$d'_{\text{aligned}}(p) = \text{ReLU}(\text{BN}(\text{Conv}(f_p))) \quad (2)$$

This process corrects erroneous depth values, resulting in a refined sparse depth map, $D_{\text{aligned}}^{(i)}$.

Simultaneously, we enhance the image features within these critical regions. For each bounding box $B_j^{(i)}$ with a predicted class label k , the corresponding image features are amplified by a class-specific hyperparameter α_k . This enhancement is applied to all pixels p within the bounding box $B_j^{(i)}$ and across all C feature channels. The operation is defined as:

$$F_{\text{enhanced}}(p, c) = \alpha_k \cdot F_{\text{img}}(p, c) \quad (3)$$

Here, the value of α_k is a class-specific hyperparameter, set based on the object’s typical size. The underlying principle is that smaller objects require a stronger feature boost to ensure their representation is not neglected during fusion. Consequently, classes like pedestrians and traffic cones are assigned a higher α_k , whereas larger classes such as buses and trucks receive a more moderate value. This allows for a more targeted enhancement, tailoring the amplification intensity to the specific characteristics of each object category.

Algorithm 1: Structural Depth Smoothing via Neighbor Concatenation

Input: Visible points $\mathcal{V} = \{v_i \mid v_i = (u_i, v_i, d_i)\}$

Parameter: Total neighbor search count $K_s = 10$

Output: Smoothed depths \mathcal{D}'

- 1: Initialize empty set \mathcal{D}' {For smoothed depths}
- 2: Extract 2D coordinates: $\mathcal{V}_{xy} \leftarrow \{(u_i, v_i) \mid v_i \in \mathcal{V}\}$
- 3: Construct KD-Tree \mathcal{T} over \mathcal{V}_{xy} {Spatial indexing}
- 4: **for** each point $v_i = (u_i, v_i, d_i) \in \mathcal{V}$ **do**
- 5: Find K_s nearest neighbors: $\mathcal{N}_i \leftarrow \text{kNN}(v_i, \mathcal{T}, K_s)$
- 6: Extract neighbor depths: $\mathcal{D}_{\mathcal{N}_i} \leftarrow \{d_j \mid v_j \in \mathcal{N}_i\}$
- 7: Sort neighbor depths: $\mathcal{D}_{\text{sorted}} \leftarrow \text{sort}(\mathcal{D}_{\mathcal{N}_i})$
- 8: Select 2 min and 2 max depth neighbors:
- 9: $\mathcal{D}_{\text{critical}} \leftarrow \{\mathcal{D}_{\text{sorted}}[0], \mathcal{D}_{\text{sorted}}[1], \mathcal{D}_{\text{sorted}}[-2], \mathcal{D}_{\text{sorted}}[-1]\}$
- 10: Concatenate original and critical depths:
- 11: $f_i \leftarrow \text{concat}(d_i, \mathcal{D}_{\text{critical}})$ {Create 5-channel feature}
- 12: Process through convolutional block:
- 13: $d'_i \leftarrow \text{ReLU}(\text{BN}(\text{Conv}(f_i)))$
- 14: $\mathcal{D}' \leftarrow \mathcal{D}' \cup \{d'_i\}$
- 15: **end for**
- 16: **return** \mathcal{D}'

These enhanced features are then processed through a Squeeze-and-Excitation (SE) block to adaptively recalibrate channel-wise feature responses, producing the final enhanced image features $F_{\text{enhanced}}^{(i)}$. This ensures that the network can learn to dynamically emphasize more informative channels for each class-specific enhancement.

Discontinuity Aware Geometric Fusion (DAGF)

The Discontinuity Aware Geometric Fusion (DAGF) module is engineered to generate a dense and structurally aware depth representation, which serves as a guide for the final depth estimation. For each camera view i , it utilizes two inputs: the original sparse depth map, denoted as $D_{\text{raw}}^{(i)}$, and a

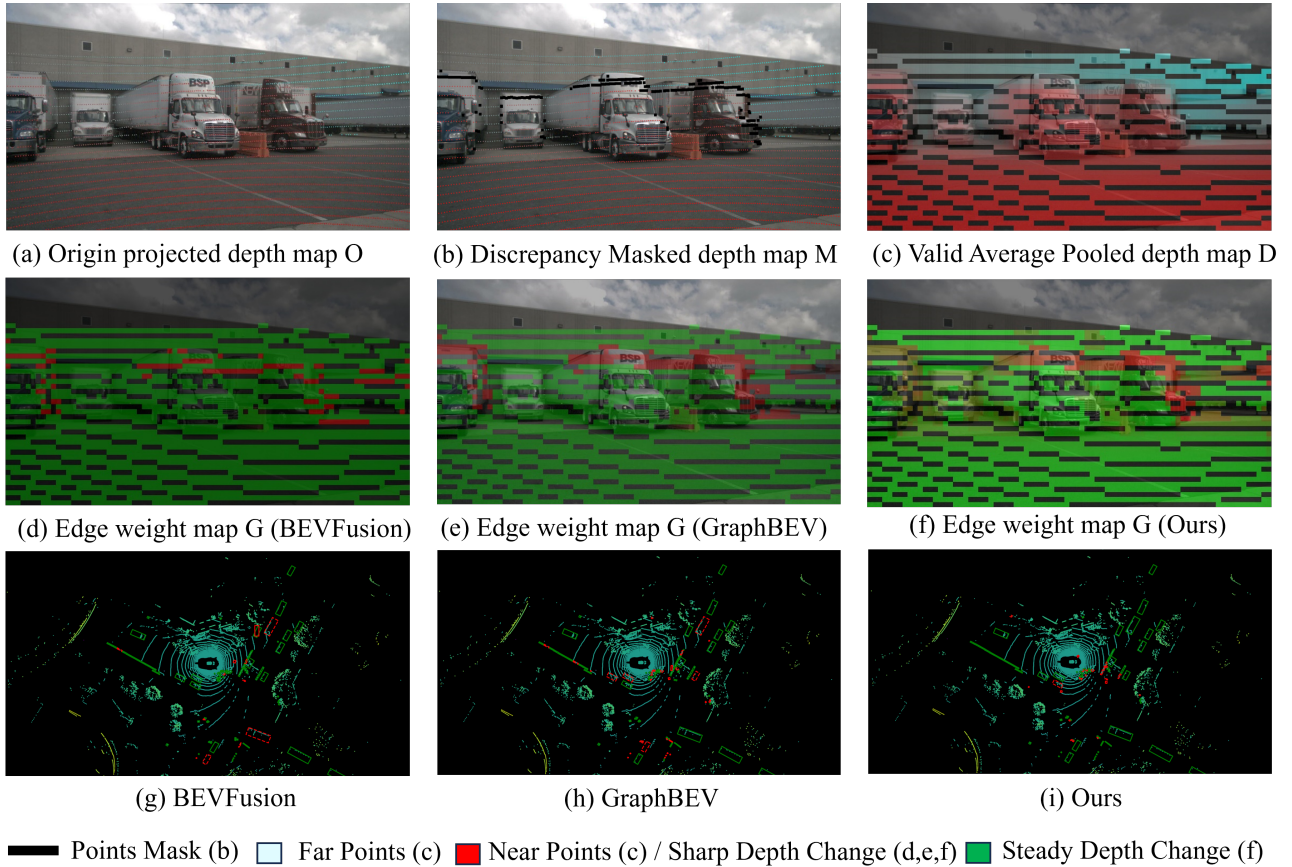


Figure 4: (a) Represents the original projected depth. (b) Represents the projected depth after applying Discrepancy Masking. (c) Shows the block-wise depth map after Block-based Densification; (d), (e), and (f) are the final depth change magnitude maps of different methods after Block-based Gradient Extraction. (g), (h) and (i) are visualization of detection results, in which green boxes are True Positives (TP), solid red boxes are False Positives (FP), and dashed red boxes are False Negatives (FN).

refined sparse depth map, $D_{\text{aligned}}^{(i)}$, which is produced by the Prior Guided Depth Calibration (PGDC) module. The module’s operation is structured as a sequential pipeline.

First, to mitigate noise via **Discrepancy Masking**, a discrepancy map $\Delta^{(i)}$ is computed. This map is defined as the absolute difference between the raw and aligned depth maps:

$$\Delta^{(i)} = |D_{\text{raw}}^{(i)} - D_{\text{aligned}}^{(i)}| \quad (4)$$

Pixels where this discrepancy surpasses a predefined threshold τ are considered unreliable and subsequently masked out from $D_{\text{aligned}}^{(i)}$. This process yields a cleaner, but still sparse, depth map, $M^{(i)}$, where the value of a pixel at coordinates (u, v) is given by:

$$M^{(i)}(u, v) = \begin{cases} D_{\text{aligned}}^{(i)}(u, v) & \text{if } \Delta^{(i)}(u, v) \leq \tau \\ 0 & \text{if } \Delta^{(i)}(u, v) > \tau \end{cases} \quad (5)$$

Next, we perform **Block-based Densification and Gradient Extraction**. The sparse map $M^{(i)}$ is divided into non-overlapping 20×20 blocks. For each block, we compute two key statistics from the valid (non-zero) points within it:

1. **Average Depth (d_{avg}):** The mean of all valid depth values in the block. This captures the block’s general distance and is used for densification.
2. **Maximum Gradient (g_{max}):** The maximum local depth discontinuity within the block. This is found by first calculating an individual gradient for each point in the block (as the max depth difference to its neighbors), and then taking the maximum of these individual gradients.

These two statistics are then broadcast to all pixels within their respective blocks, creating a densified depth map $D_{\text{dense}}^{(i)}$ and a densified gradient map $G_{\text{dense}}^{(i)}$. The visualization of these is shown in Figure 4, in which we also show the visualization of comparison between our method and others. Our method effectively addresses the misalignment between LiDAR and camera images. Furthermore, in regions with gradual depth changes, it successfully preserves relevant depth information without over-smoothing.

The ultimate output of the **Discontinuity Aware Geometric Fusion (DAGF)** module for each view is a multi-channel feature map, $F_{\text{FA}}^{(i)} \in \mathbb{R}^{H \times W \times 2}$. This feature map is formed

by concatenating the two dense maps:

$$F_{\text{FA}}^{(i)} = [D_{\text{dense}}^{(i)} \oplus G_{\text{dense}}^{(i)}] \quad (6)$$

where \oplus denotes concatenation along the channel dimension. This combined representation provides both smoothed depth information and explicit boundary-aware structural cues to the subsequent **Structural Guidance Depth Modulator (SGDM)**.

The features generated by Discontinuity Aware Geometric Fusion (DAGF) guide final depth prediction, $\hat{D}^{(i)}$, from SGDM. The training is supervised by a composite loss function that leveraged both the dense map and the gradient map.

Focal Loss. We use the densified map $D_{\text{dense}}^{(i)}$ as direct supervision for the predicted depth $\hat{D}^{(i)}$. The Focal Loss, $\mathcal{L}_{\text{focal}}$, is the average of a per-pixel loss term, $l_{\text{focal}}(u, v)$, over all valid pixels:

$$\mathcal{L}_{\text{focal}} = \frac{1}{|\mathcal{V}|} \sum_{(u,v) \in \mathcal{V}} l_{\text{focal}}(u, v) \quad (7)$$

The per-pixel term is defined as $l_{\text{focal}}(u, v) = \text{FL}(\hat{D}^{(i)}(u, v), D_{\text{dense}}^{(i)}(u, v))$. Here, \mathcal{V} is the set of all pixel coordinates with a valid (non-zero) depth, and $\text{FL}(\cdot, \cdot)$ denotes the Focal Loss function.

Edge-Critical Loss. To enforce sharp structural boundaries, the **Edge-Critical Loss**, $\mathcal{L}_{\text{edge}}$, reuses the per-pixel term $l_{\text{focal}}(u, v)$ from the Focal Loss. It introduces a weight from the gradient map, $G^{(i)}(u, v)$, to amplify the penalty at depth discontinuities:

$$\mathcal{L}_{\text{edge}} = \frac{1}{|\mathcal{V}|} \sum_{(u,v) \in \mathcal{V}} G^{(i)}(u, v) \cdot l_{\text{focal}}(u, v) \quad (8)$$

This formulation compels the network to prioritize accuracy in regions critical to structural integrity. The final training objective is a composite loss, combining these two depth-specific losses with the standard classification and bounding box regression losses:

$$\mathcal{L}_{\text{total}} = \mathcal{L}_{\text{focal}} + \mathcal{L}_{\text{edge}} + \mathcal{L}_{\text{cls}} + \mathcal{L}_{\text{box}} \quad (9)$$

Structural Guidance Depth Modulator (SGDM)

As shown in Figure 2(b), our Structural Guidance Depth Modulator (SGDM) is designed for multi-modal depth estimation, intelligently integrating visual features from the camera with geometric data from our processed depth representation. The architecture first processes camera and depth features through parallel convolutional, batch normalization, and ReLU layers, while a key residual connection preserves the original camera feature stream. These encoded features are then concatenated and fed into a gated attention mechanism, where a dynamically generated spatial attention map, created via a convolutional path and a Sigmoid function modulating a parallel feature stream. Recognizing that the fusion process can dilute the rich semantic information inherent in the camera features, we introduce a residual connection. This architecture enables the network to recover and reinforce the original semantic context. The output of this module is a discrete probability distribution over a set of predefined depth bins for each pixel.

Experiments

Dataset And Metrics

Our experiments utilize large-scale multimodal autonomous driving dataset: nuScenes. The nuScenes dataset (Caesar et al. 2020) comprises 1,000 diverse urban scenes (approximately 20 seconds each) collected across Boston and Singapore. It features 1.4 million camera images, 390,000 LiDAR sweeps, 1.4 million RADAR sweeps, and 1.4 million annotated 3D bounding boxes across 23 object classes (e.g., vehicles, pedestrians, cyclists), supplemented with precise attributes (velocity, visibility) and HD maps. Evaluation follows the benchmark’s primary metrics: mean Average Precision (mAP) and the nuScenes Detection Score (NDS).

Implementation Details

The LiDAR branch utilizes TransFusion-L (Bai et al. 2022) for feature encoding to generate Bird’s Eye View (BEV) features. Simultaneously, the camera branch processes input images resized and cropped to 448x800 resolution through a Swin Transformer backbone (Liu et al. 2021) with head counts of 3, 6, 12, and 24, followed by multi-scale feature fusion using FPN. For 2D object detection, a YOLOv9 (Wang, Yeh, and Mark Liao 2024) head is implemented. This combination provides a highly efficient and accurate detector, making it suitable for generating robust 2D priors. The LSS (Phillion and Fidler 2020) configuration defines frustum ranges with X: [-54m, 54m, 0.3m], Y: [-54m, 54m, 0.3m], Z: [-10m, 10m, 20m], and depth: [1m, 60m, 0.5m]. We implement our network in PyTorch using the open-sourced MMDetection3D, training it on eight 4090 GPUs. Latency is measured on one 4090 GPU.

Comparison Results

We evaluate our proposed framework against a comprehensive set of recent state-of-the-art (SOTA) 3D object detection methods on the challenging, large-scale benchmark: nuScenes. As detailed in Table 1, our method achieves a new state-of-the-art performance on the nuScenes validation set, reaching **71.5% mAP** and **73.6% NDS** with negligible increment of inference time. This result surpasses previous leading methods, including GraphBEV (Song et al. 2024a) (70.1% mAP, 72.9% NDS), BEVDiffuser (Ye et al. 2025) (69.2% mAP, 71.9% NDS), and the strong BEVFusion-PKU (Liu et al. 2023) baseline (67.9% mAP, 71.0% NDS). Our approach demonstrates consistently superior performance across the majority of object classes, notably achieving the highest AP scores for critical categories such as **Car (89.8%)**, **Truck (68.5%)**, **Motorcycle (80.5%)**, and **Pedestrian (90.1%)**. Significantly, we observe a substantial improvement in challenging classes like **Construction Vehicle (35.1%)** and **Bicycle (68.3%)**, underscoring our model’s enhanced robustness in handling diverse and difficult-to-detect objects by effectively mitigating feature misalignment.

Ablation Study

We adopt BEVFusion-PKU (Liang et al. 2022) as baseline to evaluate our proposed modules. As shown in Table 2, each module individually improves performance. Our

Method	mAP	NDS	C	T	CV	B	Tr	Ba	M	Bi	P	TC
TransFusion-L (CVPR 22) (Bai et al. 2022)	65.5	70.2	86.2	54.8	26.5	70.1	42.3	72.1	69.8	53.9	86.4	70.3
SAFDNet (CVPR 24) (Zhang et al. 2024)	66.3	71.0	87.6	60.8	26.6	78.0	43.5	69.7	75.5	58.0	87.8	75.0
BEVFusion-PKU (NeurIPS 22) (Liu et al. 2023)	67.9	71.0	87.3	59.8	28.9	73.5	41.2	73.8	74.6	59.8	85.4	68.2
LION-Mamba (NeurIPS 24) (Liu et al. 2024b)	68.0	72.1	87.9	64.9	28.5	77.6	44.4	71.6	75.6	59.4	89.6	80.8
FSHNet (CVPR 25) (Liu et al. 2025)	68.1	71.7	88.7	61.4	26.3	79.3	47.8	72.3	76.7	60.5	89.3	78.6
BEVFusion-MIT (ICRA 23) (Liang et al. 2022)	68.5	71.4	88.2	61.7	30.2	75.1	41.5	72.5	76.3	64.2	87.5	81.0
UniMamba (CVPR 25) (Jin et al. 2025)	68.5	72.6	88.7	64.7	28.7	79.7	47.9	72.3	74.6	59.1	89.7	79.5
M3Net (AAAI 25) (Chen et al. 2025)	69.0	72.4	89.0	64.5	30.3	77.9	47.5	73.2	76.5	61.4	89.2	80.4
BEVDiffuser (CVPR 25) (Ye et al. 2025)	69.2	71.9	88.5	63.5	31.0	75.3	46.2	73.2	77.5	62.8	87.9	80.5
GraphBEV (ECCV 24) (Song et al. 2024a)	70.1	72.9	89.8	64.2	31.2	75.8	43.5	75.6	79.3	66.3	88.6	80.9
Ours	71.5	73.6	89.8	68.5	35.1	77.2	45.5	78.0	80.5	68.3	90.1	82.0

Table 1: Performance comparison of 3D object detection methods on the nuScenes validation set across 10 classes: Car (C), Truck (T), Construction Vehicle (CV), Bus (B), Trailer (Tr), Barrier (Ba), Motorcycle (M), Bicycle (Bi), Pedestrian (P), and Traffic Cone (TC).

DAGF module relies on PGDC; for the DAGF-only ablation, we modified it to use the original depth map directly. The results reveal a strong synergistic effect between PGDC and DAGF, where their combined gain exceeds the sum of their individual contributions.

PGDC	DAGF	SGDM	mAP (%)	NDS (%)
×	×	×	67.9	71.0
✓	×	✓	69.8	72.5
×	✓	✓	69.0	71.6
✓	✓	✓	71.5	73.6

Table 2: Ablation study of our three proposed modules. The baseline uses none of our components. All other configurations use our SGDM module to process inputs from the enabled data-processing modules (PGDC, DAGF).

To further analyse component contributions, Table 3 presents a granular ablation. We incrementally test PGDC’s functions, the Depth Align Module (DAM) and the Feature Enhance Module (FEM), and DAGF’s representations (D_{dense} and G_{dense}). The results show DAM provides the most significant initial boost. FEM offers a further gain, followed by the dense depth representation. Finally, the gradient representation pushes the model to its peak performance.

DAM	FEM	D_{dense}	G_{dense}	mAP (%)	NDS (%)
×	×	×	×	67.9	71.0
✓	×	×	×	69.4	72.1
✓	✓	×	×	69.8	72.5
✓	✓	✓	×	70.8	73.1
✓	✓	✓	✓	71.5	73.6

Table 3: Granular ablation study. DAM: Depth Align Module. FEM: Feature Enhance Module. D_{dense} : Using the dense depth representation from DAGF. G_{dense} : Using the dense gradient representation from DAGF.

Finally, to isolate the impact of 2D detector accuracy, Table 4 shows an ablation study on 2D prior quality. We com-

pare scenarios with no priors, noisy priors, realistic priors (YOLOv9), and perfect ground truth priors. The noisy condition refers to the YOLOv9 detection results with a synthetically introduced 10% false negative rate (missed detections) and a 10% false positive rate (incorrect detections). The results demonstrate that performance scales with the quality of the 2D priors, and our method with a realistic detector nearly closes the gap to the ceiling set by perfect information. For more ablation results about hyperparameters, please refer to the Appendix.

2D Prior Source	mAP (%)	NDS (%)
No 2D Priors	69.0	71.6
Noisy 2D Priors	70.3	72.5
Realistic 2D Priors	71.5	73.6
Ground Truth 2D Priors	73.5	74.2

Table 4: Ablation study on impact of 2D detectors. We test scenarios with no 2D priors, noisy priors, realistic priors from YOLOv9, and perfect priors from ground truth.

Conclusion

In this work, we address the critical issue of LiDAR-camera feature misalignment, most severe at object-background boundaries due to depth-dependent projection errors. To proactively correct these errors stemming from calibration and motion, our framework introduces three novel components. Prior Guided Depth Calibration (PGDC) leverages 2D detection priors to correct depth supervision in critical regions. Discontinuity Aware Geometric Fusion (DAGF) then creates a dense, structurally aware representation. Finally, the Structural Guidance Depth Modulator (SGDM) intelligently fuses these visual and geometric cues to predict a highly accurate depth distribution for view transformation, effectively mitigating artifacts in the final BEV space. Experimental validation on nuScenes validation dataset demonstrates state-of-the-art performance with 71.5% mAP and 73.6% NDS. Our method yields a 3.6% gain in mAP and a 2.6% gain in NDS, while only adding 15ms of latency.

References

- Bai, X.; Hu, Z.; Zhu, X.; Huang, Q.; Chen, Y.; Fu, H.; and Tai, C.-L. 2022. Transfusion: Robust lidar-camera fusion for 3d object detection with transformers. In *Proceedings of the IEEE/CVF conference on computer vision and pattern recognition*, 1090–1099.
- Caesar, H.; Bankiti, V.; Lang, A. H.; Vora, S.; Liong, V. E.; Xu, Q.; Krishnan, A.; Pan, Y.; Baldan, G.; and Beijbom, O. 2020. nuscenes: A multimodal dataset for autonomous driving. In *Proceedings of the IEEE/CVF conference on computer vision and pattern recognition*, 11621–11631.
- Cai, Q.; Pan, Y.; Yao, T.; Ngo, C.-W.; and Mei, T. 2023. Objectfusion: Multi-modal 3d object detection with object-centric fusion. In *Proceedings of the IEEE/CVF International Conference on Computer Vision*, 18067–18076.
- Chen, X.; Shi, S.; Ma, T.; Zhou, J.; See, S.; Cheung, K. C.; and Li, H. 2025. M3net: Multimodal multi-task learning for 3d detection, segmentation, and occupancy prediction in autonomous driving. In *Proceedings of the AAAI Conference on Artificial Intelligence*, volume 39, 2275–2283.
- Chen, Y.; Liu, J.; Zhang, X.; Qi, X.; and Jia, J. 2023. Largekernel3d: Scaling up kernels in 3d sparse cnns. In *Proceedings of the IEEE/CVF conference on computer vision and pattern recognition*, 13488–13498.
- Chen, Z.; Li, Z.; Zhang, S.; Fang, L.; Jiang, Q.; and Zhao, F. 2022. Deformable feature aggregation for dynamic multi-modal 3D object detection. In *European conference on computer vision*, 628–644. Springer.
- Ge, C.; Chen, J.; Xie, E.; Wang, Z.; Hong, L.; Lu, H.; Li, Z.; and Luo, P. 2023. Metabev: Solving sensor failures for 3d detection and map segmentation. In *Proceedings of the IEEE/CVF International Conference on Computer Vision*, 8721–8731.
- Guo, K.; and Ling, Q. 2025. PromptDet: A Lightweight 3D Object Detection Framework with LiDAR Prompts. In *Proceedings of the AAAI Conference on Artificial Intelligence*, volume 39, 3266–3274.
- Huang, J.; and Huang, G. 2022. Bevdet4d: Exploit temporal cues in multi-camera 3d object detection. *arXiv preprint arXiv:2203.17054*.
- Jin, X.; Su, H.; Liu, K.; Ma, C.; Wu, W.; Hui, F.; and Yan, J. 2025. UniMamba: Unified Spatial-Channel Representation Learning with Group-Efficient Mamba for LiDAR-based 3D Object Detection. In *Proceedings of the Computer Vision and Pattern Recognition Conference*, 1407–1417.
- Lang, A. H.; Vora, S.; Caesar, H.; Zhou, L.; Yang, J.; and Beijbom, O. 2019. Pointpillars: Fast encoders for object detection from point clouds. In *Proceedings of the IEEE/CVF conference on computer vision and pattern recognition*, 12697–12705.
- Li, Y.; Ge, Z.; Yu, G.; Yang, J.; Wang, Z.; Shi, Y.; Sun, J.; and Li, Z. 2023. Bevdepth: Acquisition of reliable depth for multi-view 3d object detection. In *Proceedings of the AAAI conference on artificial intelligence*, volume 37, 1477–1485.
- Li, Z.; Wang, F.; and Wang, N. 2021. Lidar r-cnn: An efficient and universal 3d object detector. In *Proceedings of the IEEE/CVF conference on computer vision and pattern recognition*, 7546–7555.
- Liang, T.; Xie, H.; Yu, K.; Xia, Z.; Lin, Z.; Wang, Y.; Tang, T.; Wang, B.; and Tang, Z. 2022. Bevfusion: A simple and robust lidar-camera fusion framework. *Advances in Neural Information Processing Systems*, 35: 10421–10434.
- Liu, L.; Song, Z.; Xia, Q.; Jia, F.; Jia, C.; Yang, L.; Gong, Y.; and Pan, H. 2024a. Sparsedet: a simple and effective framework for fully sparse lidar-based 3D object detection. *IEEE Transactions on Geoscience and Remote Sensing*.
- Liu, S.; Cui, M.; Li, B.; Liang, Q.; Hong, T.; Huang, K.; and Shan, Y. 2025. FSHNet: Fully Sparse Hybrid Network for 3D Object Detection. In *Proceedings of the Computer Vision and Pattern Recognition Conference*, 8900–8909.
- Liu, Z.; Hou, J.; Wang, X.; Ye, X.; Wang, J.; Zhao, H.; and Bai, X. 2024b. Lion: Linear group rnn for 3d object detection in point clouds. *Advances in Neural Information Processing Systems*, 37: 13601–13626.
- Liu, Z.; Huang, T.; Li, B.; Chen, X.; Wang, X.; and Bai, X. 2022. EPNet++: Cascade bi-directional fusion for multi-modal 3D object detection. *IEEE transactions on pattern analysis and machine intelligence*, 45(7): 8324–8341.
- Liu, Z.; Lin, Y.; Cao, Y.; Hu, H.; Wei, Y.; Zhang, Z.; Lin, S.; and Guo, B. 2021. Swin Transformer: Hierarchical Vision Transformer using Shifted Windows. In *2021 IEEE/CVF International Conference on Computer Vision (ICCV)*.
- Liu, Z.; Tang, H.; Amini, A.; Yang, X.; Mao, H.; Rus, D. L.; and Han, S. 2023. Bevfusion: Multi-task multi-sensor fusion with unified bird’s-eye view representation. In *2023 IEEE international conference on robotics and automation (ICRA)*, 2774–2781. IEEE.
- Lu, Y.; Ma, X.; Yang, L.; Zhang, T.; Liu, Y.; Chu, Q.; Yan, J.; and Ouyang, W. 2021. Geometry uncertainty projection network for monocular 3d object detection. In *Proceedings of the IEEE/CVF International Conference on Computer Vision*, 3111–3121.
- Miao, Z.; Chen, J.; Pan, H.; Zhang, R.; Liu, K.; Hao, P.; Zhu, J.; Wang, Y.; and Zhan, X. 2021. Pvgnet: A bottom-up one-stage 3d object detector with integrated multi-level features. In *Proceedings of the IEEE/CVF conference on computer vision and pattern recognition*, 3279–3288.
- Philion, J.; and Fidler, S. 2020. Lift, splat, shoot: Encoding images from arbitrary camera rigs by implicitly unprojecting to 3d. In *Computer Vision—ECCV 2020: 16th European Conference, Glasgow, UK, August 23–28, 2020, Proceedings, Part XIV 16*, 194–210. Springer.
- Pu, F.; Wang, Y.; Deng, J.; and Yang, W. 2025. Monodgpp: Monocular 3D object detection with decoupled-query and geometry-error priors. In *Proceedings of the Computer Vision and Pattern Recognition Conference*, 6520–6530.
- Qi, C. R.; Liu, W.; Wu, C.; Su, H.; and Guibas, L. J. 2018. Frustum pointnets for 3d object detection from rgb-d data. In *Proceedings of the IEEE conference on computer vision and pattern recognition*, 918–927.
- Qi, C. R.; Yi, L.; Su, H.; and Guibas, L. J. 2017. Pointnet++: Deep hierarchical feature learning on point sets in a metric

- space. *Advances in neural information processing systems*, 30.
- Reading, C.; Harakeh, A.; Chae, J.; and Waslander, S. L. 2021. Categorical depth distribution network for monocular 3d object detection. In *Proceedings of the IEEE/CVF conference on computer vision and pattern recognition*, 8555–8564.
- Song, Z.; Wei, H.; Bai, L.; Yang, L.; and Jia, C. 2023a. GraphAlign: Enhancing accurate feature alignment by graph matching for multi-modal 3D object detection. In *Proceedings of the IEEE/CVF international conference on computer vision*, 3358–3369.
- Song, Z.; Wei, H.; Jia, C.; Xia, Y.; Li, X.; and Zhang, C. 2023b. VP-Net: Voxels as points for 3-D object detection. *IEEE Transactions on Geoscience and Remote Sensing*, 61: 1–12.
- Song, Z.; Yang, L.; Xu, S.; Liu, L.; Xu, D.; Jia, C.; Jia, F.; and Wang, L. 2024a. Graphbev: Towards robust bev feature alignment for multi-modal 3d object detection. In *European Conference on Computer Vision*, 347–366. Springer.
- Song, Z.; Zhang, G.; Liu, L.; Yang, L.; Xu, S.; Jia, C.; Jia, F.; and Wang, L. 2024b. RoboFusion: Towards robust multi-modal 3D object detection via SAM. *arXiv preprint arXiv:2401.03907*.
- Wang, C.; Ma, C.; Zhu, M.; and Yang, X. 2021. Pointaugmenting: Cross-modal augmentation for 3d object detection. In *Proceedings of the IEEE/CVF conference on computer vision and pattern recognition*, 11794–11803.
- Wang, C.-Y.; Yeh, I.-H.; and Mark Liao, H.-Y. 2024. Yolov9: Learning what you want to learn using programmable gradient information. In *European conference on computer vision*, 1–21. Springer.
- Wang, J.; Li, F.; An, Y.; Zhang, X.; and Sun, H. 2024. Towards robust lidar-camera fusion in bev space via mutual deformable attention and temporal aggregation. *IEEE Transactions on Circuits and Systems for Video Technology*.
- Wang, Y.; Guizilini, V. C.; Zhang, T.; Wang, Y.; Zhao, H.; and Solomon, J. 2022. Detr3d: 3d object detection from multi-view images via 3d-to-2d queries. In *Conference on Robot Learning*, 180–191. PMLR.
- Ye, X.; Yaman, B.; Cheng, S.; Tao, F.; Mallik, A.; and Ren, L. 2025. BEVDiffuser: Plug-and-Play Diffusion Model for BEV Denoising with Ground-Truth Guidance. In *Proceedings of the Computer Vision and Pattern Recognition Conference*, 1495–1504.
- Yin, T.; Zhou, X.; and Krähenbühl, P. 2021. Multimodal virtual point 3d detection. *Advances in Neural Information Processing Systems*, 34: 16494–16507.
- Yu, K.; Tao, T.; Xie, H.; Lin, Z.; Liang, T.; Wang, B.; Chen, P.; Hao, D.; Wang, Y.; and Liang, X. 2023. Benchmarking the robustness of lidar-camera fusion for 3d object detection. In *Proceedings of the IEEE/CVF Conference on Computer Vision and Pattern Recognition*, 3188–3198.
- Zhang, G.; Chen, J.; Gao, G.; Li, J.; Liu, S.; and Hu, X. 2024. Safdnet: A simple and effective network for fully sparse 3d object detection. In *Proceedings of the IEEE/CVF Conference on Computer Vision and Pattern Recognition*, 14477–14486.
- Zhang, J.; Zhang, Y.; Qi, Y.; Fu, Z.; Liu, Q.; and Wang, Y. 2025. Geobev: Learning geometric bev representation for multi-view 3d object detection. In *Proceedings of the AAAI Conference on Artificial Intelligence*, volume 39, 9960–9968.
- Zhou, Y.; and Tuzel, O. 2018. Voxelnet: End-to-end learning for point cloud based 3d object detection. In *Proceedings of the IEEE conference on computer vision and pattern recognition*, 4490–4499.